Quantization Effects in the Photocurrent Spectroscopy of Superlattice Electrodes

A. J. Nozik,* B. R. Thacker, J. A. Turner, and J. M. Olson

*Contribution from the Solar Energy Research Institute, Golden, Colorado 80401.
Received July 29, 1985*

Abstract: Strained-layer superlattices of $GaAs/GaAs_{1-x}P_x$, $x \approx 0.5$, have been investigated as photoelectrodes in photoelectrochemical cells. Pronounced structure in the photocurrent spectra are observed that can be resolved into a series of Gaussian peaks that match the expected transitions between the theoretical energy levels of the GaAs quantum wells. The photocurrent spectra of various samples with the same quantum well width show marked variation in peak intensities, but with about the same peak positions. The sign of the photocurrent and the peak intensities depend upon photon energy, electrode potential, and electrolyte redox potential. The quantum yields were much higher for superlattices with 50-Å barriers compared to 250-Å barriers. A major conclusion is that electron injection into the electrolyte occurs from higher lying energy levels in the quantum wells, constituting a hot electron injection process. A qualitative model of the behavior of superlattice electrodes in photoelectrochemical cells is presented.

Introduction

Novel and interesting effects in semiconductors that arise from the quantization of the energy levels of charge carriers (electrons and positive holes) confined to potential wells of very small dimensions are under intense investigation.[1-13] The phenomena arise when the size of the potential well becomes comparable to the de Broglie wavelength of the charge carriers; the situation is generally described by the well-known quantum mechanics of a "particle in a box". The size of the semiconductor structures required to produce quantization effects depends upon the effective masses of the electrons and holes but typically ranges from about 25 to 250 Å.

Three regimes can be considered depending on whether the potential wells are small in one, two, or three dimensions. For the latter, the systems under study consist primarily of colloidal semiconductor particles suspended in a liquid matrix.[8-11] Two-dimensional systems have also been prepared and are called

quantum wires.[12,13] However, the vast majority of work on quantum size effects has been done on one-dimensional systems in the form of multiple quantum wells (MQW) and superlattices (SL).[1-7] In one configuration, these structures consist of alternating thin layers of two semiconductors with two different band gaps such that the small gap semiconductor forms a series of square potential wells and the large gap semiconductor forms a series of potential barriers. Potential wells for both conduction band electrons and valence band holes are formed, and the respective heights of these two wells depend upon the offsets of the positions of the conduction and valence band edges for the two semiconductors. The well widths and barrier thicknesses, as well as the number of wells, can be controlled by the thin film depostion processes.

If the charge carriers in adjacent wells cannot communicate because the potential barriers are too thick, then the wells are isolated and the structure is termed multiple quantum wells (MQW). The energy levels in the MQW structure consist of a finite series of discrete and narrow states that are described by the quantum mechanics of particles confined to a one-dimensional square well. If the charge carriers can communicate with adjacent wells via tunnelling processes through sufficiently thin potential barriers, then the wells become quantum mechanically coupled and the wave functions extend through the whole layered structure. This leads to the formation of a series of minibands for electrons and holes with band widths and spacings determined by the dimensions of the semiconductor layers. Such structures are termed superlattices (SL). If the alternating semiconductor layers are not lattice matched, large strains develop at the interfaces and these superlattices are labeled strained-layer superlattices (SLS); both strained and unstrained superlattices exhibit unique properties and are under investigation.

Another configuration that we will not be concerned with in the present work consists of alternating thin layers of n- and p-type

(1) R. Tsu and L. Esaki, *Appl. Phys. Letts.*, **22**, 562 (1973).
(2) R. Dingle, *Festkörperprobleme*, **15**, 21 (1975).
(3) K. Ploog and G. H. Döhler, *Adv. Phys.*, **32**, 285 (1983).
(4) L. L. Chang, *J. Vac. Sci. Technol. B*, **1**, 120 (1983).
(5) G. H. Döhler, *Superlattices Microstruct.*, **1**, 279 (1985); *Sci. Am.*, **249**, 144 (1984).
(6) G. C. Osbourn, *J. Vac. Sci. Technol.*, **21**, 379 (1983).
(7) P. L. Gourley and R. M. Biefeld, *Appl. Phys. Lett.* **45**, 749 (1984).
(8) L. E. Brus, *J. Chem. Phys.*, **80**, 4403 (1984).
(9) R. Rossetti, J. L. Ellison, J. M. Gibson, and L. E. Brus, *J. Chem. Phys.*, **80**, 4464 (1984).
(10) A. J. Nozik, F. Williams, M. T. Nenandović, T. Rajh, and O. I. Mićić, *J. Phys. Chem.*, **89**, 397 (1985).
(11) A. Fojtik, H. Weller, U. Koch, and A. Henglein, *Ber. Bunsenges. Phys. Chem.*, **89**, 969 (1984).
(12) M. Laviron, P. Averbuch, H. Godfrin, and R. E. Rapp, *J. Phys. Lett.*, **44**, L-1021 (1983).
(13) P. M. Petroff, A. C. Gossard, R. A. Logan, and W. Wiegmann, *Appl. Phys. Lett.*, **44**, 635 (1982).

semiconductors of the same parent material; these are termed doping superlattices.

Various solid-state configurations of SL and MQW structures are being actively studied both for their intrinsic properties and as new types of solid-state devices.[1-7] We have recently reported initial results using superlattices for the first time as photoelecrodes in photoelectrochemical cells.[14] Very pronounced and interesting quantization effects were observed in the photocurrent spectra. In this paper we present results of a more complete study of superlattice photoelectrodes showing the effects of electrode potential, electrolyte redox potential, and barrier thickness on the quantization effects in SL photoelectrodes; a qualitative model for the observed behavior is presented.

Experimental Section

The first superlattice electrodes we studied consisted of 20 alternating layers each of GaAs and $GaAs_{1-x}P_x$ with nominal composition $x = 0.5$. The semiconductors were not deliberately doped and had carrier concentrations in the range of 10^{15} to 10^{16} cm^{-3}. The layers were each 250-Å thick, and the outer-most top layer was GaAs. This system is a SLS with GaAs wells and $GaAs_{0.5}P_{0.5}$ barriers, both 250-Å wide; the band gaps for this system are 1.42 eV for GaAs and 2.0 eV for $GaAs_{0.5}P_{0.5}$. The barrier heights for the electron wells in the conduction band and the hole wells in the valence band are reported to be 0.28 and 0.30 eV, respectively.[7,14] The SLS was grown by metalorganic chemical vapor deposition (MOCVD) with continuous flows of trimethylgallium, PH_3, and AsH_3. The growth rate and temperature were 0.1 μm/min and 750 °C, respectively. The composition of the superlattice layers was determined by calibrating the growth parameters of the MOCVD apparatus with a series of runs in which thick (2–4 μm) layers of $GaAs_{1-x}P_x$ were deposited and their chemical composition determined by electron microprobe analysis.

A 10-μm $GaAs_{1-x}P_x$ buffer layer graded from $x = 0$ to 0.25 in five equal steps was grown between the p^+-GaAs single crystal substrate and the SLS. The p^+-GaAs wafers were oriented 2° off (100) towards (110) and were cleaned prior to growth with a 6:1:1 H_2SO_4:H_2O_2:H_2O etch. The lattice mismatch of the GaAs and $GaAs_{0.5}P_{0.5}$ layers produced large strain parallel and perpendicular to the layers. Scanning electron micrographs of the SLS cross-section showed wavy but equidistant layers.[14] Two separate runs were made to produce two batches of this first SLS structure.

The second SLS structure consisted of the same configuration as described above except that the $GaAs_{0.5}P_{0.5}$ barrier thickness was 50 Å.

Photoelectrodes were prepared from the SLS samples by first cutting the wafers into smaller pieces (1 to 10 mm²), electroplating the p^+-GaAs substrate with a gold ohmic contact, and sealing all but the front SLS surface with epoxy. The electrodes were studied with no surface pretreatment in a conventional photoelectrochemical cell containing either 0.1 M $Eu(ClO_4)_3$ in 1 M $HClO_4$ or 0.2 M potassium ferricyanide in 1 M H_2SO_4. Photoaction spectra were obtained with chopped light referenced to a lock-in amplifier. The monochromator and data acquistion were both computer controlled, with all spectra recorded at 2-nm intervals. The data were normalized with respect to the lamp spectra and quantum yields obtained by measuring the light intensity with a calibrated photodiode. No corrections were made for absorption or reflection losses. The monochromatic light intensities were typically in the range of 50 to 400 μW/cm², and the photocurrent densities ranged from 2 to 25 μamps/cm².

Results reported using an energy scale were generated from the wavelength data by digitizing it into equal energy intervals of 2.5 meV with a cubic spline fitting program.

All electrode potentials reported here are vs. the standard calomel electrode (SCE).

Results

(A) General Photocurrent Behavior. The most dramatic and general effect observed with $GaAs_{0.5}P_{0.5}$ SLS photoelectrodes is pronounced and rather well-resolved structure in the photocurrent action spectra (quantum yield vs. photon energy or wavelength) at room temperature. Typical results are shown in Figure 1 for photoelectrodes at −0.8 or −1.0 V in ferricyanide electrolyte over the energy range 1.30 to 2.00 eV. All these samples had the same SLS configuration (250-Å GaAs wells and 250-Å $GaAs_{0.5}P_{0.5}$ barriers) but were taken from different runs or from different
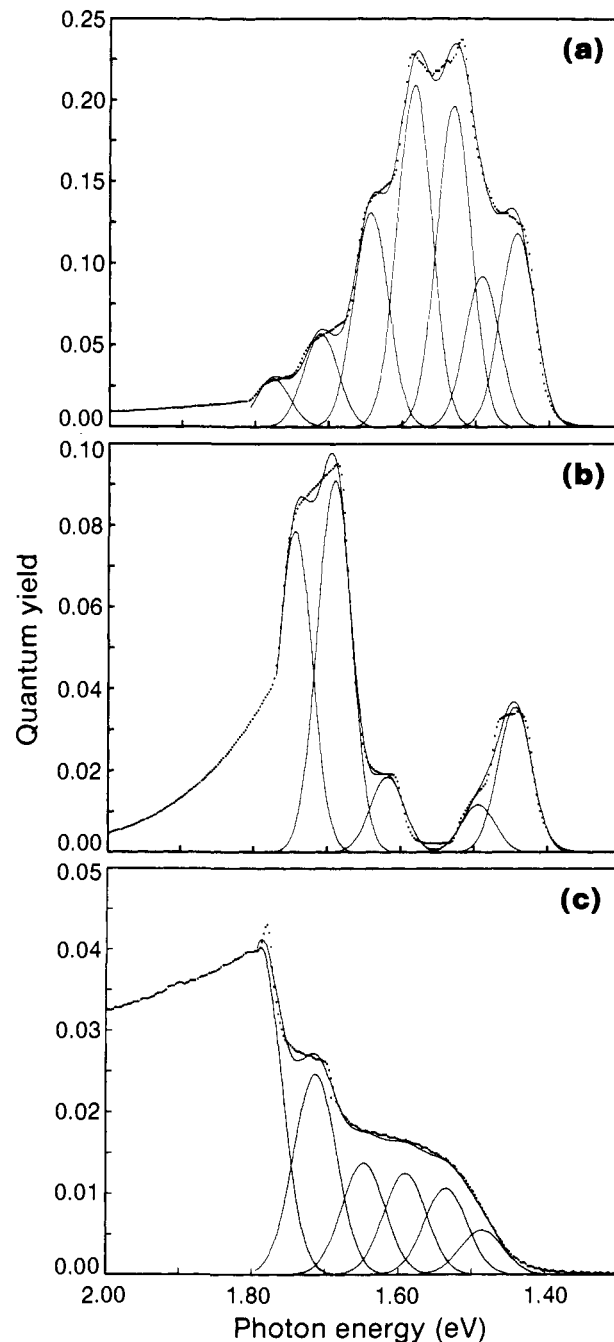
(14) A. J. Nozik, B. R. Thacker, and J. M. Olson, *Nature (London)*, **316**, 51 (1985).

Figure 1. Photocurrent spectra (eV scale) for three $GaAs/GaAs_{0.5}P_{0.5}$ SLS electrodes showing marked differences in photocurrent peak intensities with approximately constant peak positions. All spectra were obtained with 0.2 M $Fe(CN)_6^{3-}$ in H_2SO_4. Electrode potentials were −1.0 V for (a) and (c) and −0.8 V for (b) vs. SCE. Solid lines are theoretical fits; dots are experimental data. Photocurrent is cathodic. For a given sample there is no significant change in spectral shape between −0.8 and −1.0 V vs. SCE.

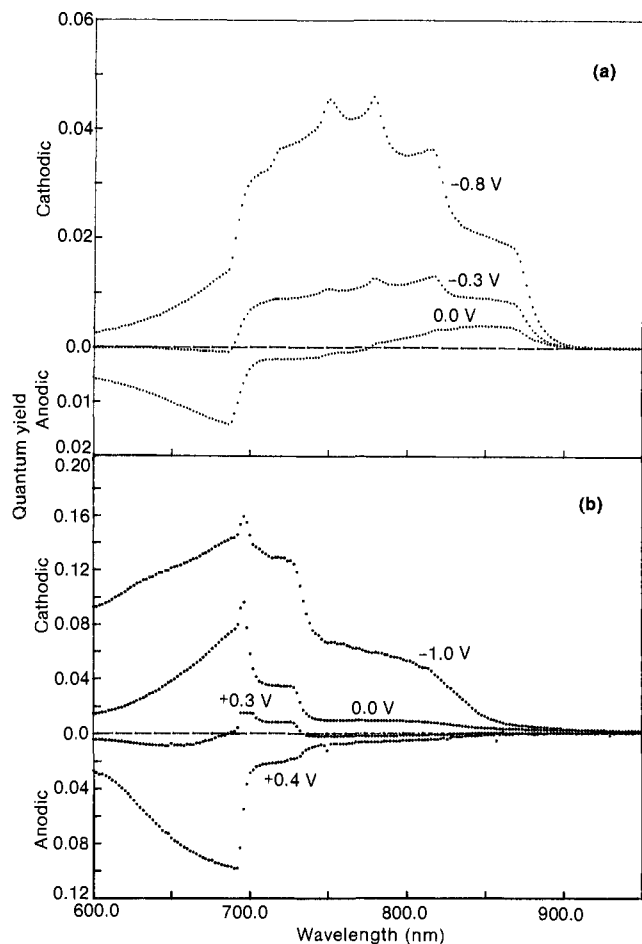regions of the SLS wafer made in the same run.

The structured cathodic photocurrent spectra could be readily fitted to a sum of Gaussian peaks constrained to a common line width. Good fits could be obtained whether the spectra were fittted with a wavelength scale or an energy scale; peak positions were also the same within 0.01 to 0.02 eV for the two scales. The fitted peak positions using the eV scale are listed in Table I.

What is especially striking about these results is that the peak intensities and net overall shape of the photocurrent spectra vary greatly among the samples, while the peak positions remain approximately constant. The average fitted line width for the spectra in Figure 1 is 50.7 meV. The maximum quantum yields at potentials of −0.8 to −1.0 V range from about 5% to 20%. The effect

Table I. Photocurrent Peak Positions for Various $GaAs/GaAs_{0.5}P_{0.5}$ SLS Electrodes with 250 Å Well Thickness

	peak positions, eV							width at half-height (meV)
sample	1	2	3	4	5	6	6'	
Figure 1a	1.44	1.49	1.53	1.58	1.64	1.71	1.77	46.9
Figure 1b	1.45	1.49			1.62	1.69	1.75	46.1
Figure 1c		1.49	1.54	1.59	1.65	1.71	1.79	59.0
Figure 3	1.44	1.48	1.53	1.59	1.65	1.71	1.78	47.8
av	1.44	1.49	1.53	1.59	1.64	1.71	1.78	50.0
theory	1.43	1.46	1.50	1.55	1.63	1.72	1.77	

Figure 3. Photocurrent spectrum of electrode used in Figure 1a with Eu^{3+} present; effect of redox potential of electrolyte on relative peak intensities is seen by comparing Figures 1a and 3. Solid lines are theoretical fits; dots are experimental data. Photocurrent is cathodic.

Figure 2. Effect of electrode potential on photocurrent spectra for two SLS samples in two electrolytes: (a) 0.1 M Eu^{3+} in $HClO_4$; (b) 0.2 M $Fe(CN)_6^{3-}$ in H_2SO_4.
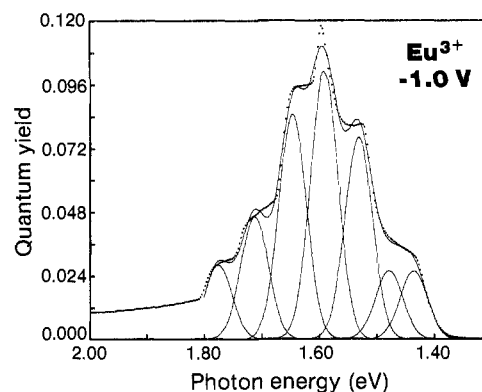
of electrode potential on the photocurrent peak intensities and overall shape are described below.

Two other consistent features of the photocurrent spectra, exemplified in Figure 1, are the sudden cutoff of peak structure at 1.8 eV (~685 nm) and a smooth photocurrent tail that extends from the 1.8-eV transition point to higher energies. The nature of this tail (shape, magnitude, and sign) depends dramatically on the SLS sample and the electrode potential (see below).

A final important feature of the photocurrent spectra is the wide variation in quantum yields at the higher energies (> ~1.65 eV). Some samples show a drastic drop in quantum yield above ~1.65 eV; other samples do not show such a drop-off (e.g., see Figure 1c), and the quantum yields remain nearly constant up to 3 eV.

The current–voltage curves for the SLS electrodes show very little dark current between 0 and −1.0 V. The photocurrent changes sign at potentials that depend upon the wavelength of photoexcitation and on the redox potential of the electrolyte; these effects are discussed in greater detail below.

Photocurrent spectra of 2-μm films of p-GaAs also grown by MOCVD showed the usual photocurrent onset at ~900 nm,

followed by a smoothly rising curve that saturates at 825 nm at quantum efficiencies of 70%.

(B) Effects of Electrode Potential. Photocurent spectra as a function of electrode potential were obtained for several samples. Figure 2 illustrates behavior over the potential range −1.0 to +0.4 V for two of the 250 Å GaAs/250 Å $GaAs_{0.5}P_{0.5}$ SLS samples; the electrolyte was Eu^{3+} in $HClO_4$ in Figure 2a and $Fe(CN)_6^{3-}$ in H_2SO_4 in Figure 2b. The striking feature of Figure 2 is the change in sign of the photocurrent at shorter wavelength that occurs at more positive electrode potentials. The first sample (**2a**) is related to that in Figure 1a; as the potential becomes more positive (less band bending) the quantum yield of the cathodic current decreases and the structure in the photocurrent spectra is diminished; at 0.0 V the photocurrent changes sign at 775 nm. The transition wavelength at 685 nm (where the structure in the photocurrent spectra suddenly disappears) does not change with potential. However, the sign and magnitude of the photocurrent tail below the transition wavelength are very sensitive to potential. As seen in Figure 2a, at −1.0 V the photocurrent tail is cathodic, at −0.4 V the photocurrent tail is essentially zero, and at 0.0 V it is anodic.

Quite different behavior is shown in Figure 2b for the second 250 Å GaAs/250 Å $GaAs_{0.5}P_{0.5}$ sample in $Fe(CN)_6^{3-}$ electrolyte at potentials of −1.0, 0.0, +0.3, and +0.4 V; this sample is related to that shown in Figure 1c. In contrast to Figure 2a, the photocurrent in Figure 2b at 0.0 V does not undergo a sign change at shorter wavelength. At +0.3 V there is a sign change at 680 nm, while at +0.4 V the photocurrent is anodic over the whole wavelength range 600–950 nm. It is notable that the cathodic and anodic spectra at 0.0 and +0.4 V show a mirror-like symmetry, with similar photocurrent structure at wavelengths >685 nm.

At potentials of −0.8 to −1.0 V, the shapes of the photocurrent spectra of the SLS electrodes for both Eu^{3+} and $Fe(CN)_6^{3-}$ electrolytes are insensitive to electrode potential.

(C) Effects of Electrolyte Redox Potential. The redox potential of the electron acceptors in the electrolyte affects the photocurrent peak intensities as well as the sign of the photocurrent in certain wavelength regions. Figure 3 shows the photocurrent spectrum of the same electrode used in Figure 1a, except that the electron acceptor is Eu^{3+} instead of $Fe(CN)_6^{3-}$. The standard redox po-

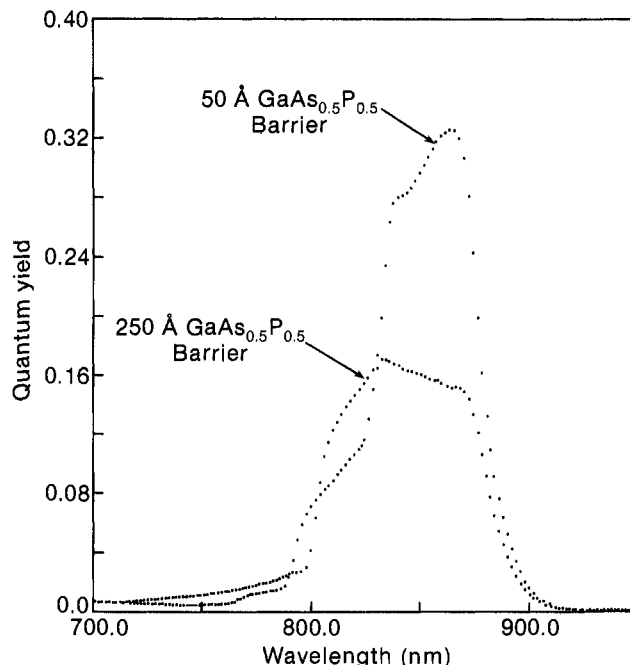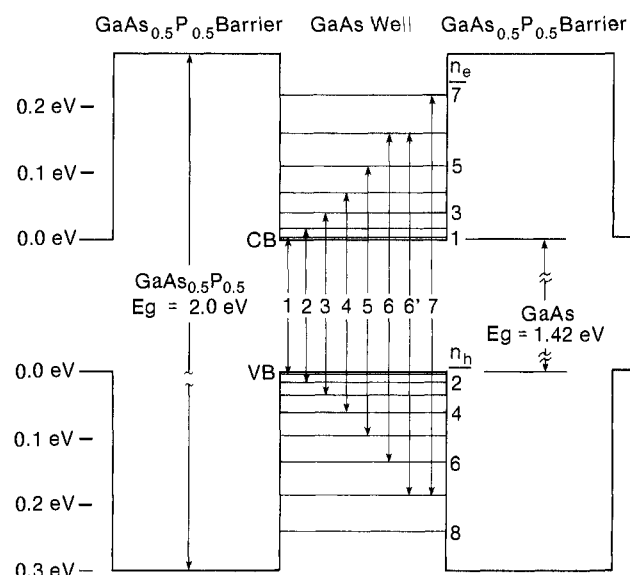**Table II.** Comparison of Relative Photocurrent Peak Intensities for Eu^{3+} and $Fe(CN)_6^{3-}$ Electron Acceptors (Figures 1a and 3) (Electrode Potential Is -1.0 V vs. SCE)

| peak | energy, eV | rel peak intensities | |
		Eu^{3+}	$Fe(CN)_6^{3-}$
1	1.44	1.00	1.00
2	1.49	1.00	0.78
3	1.53	2.95	1.66
4	1.59	3.92	1.77
5	1.65	3.30	1.11
6	1.71	1.80	0.48
6'	1.78	1.09	0.25
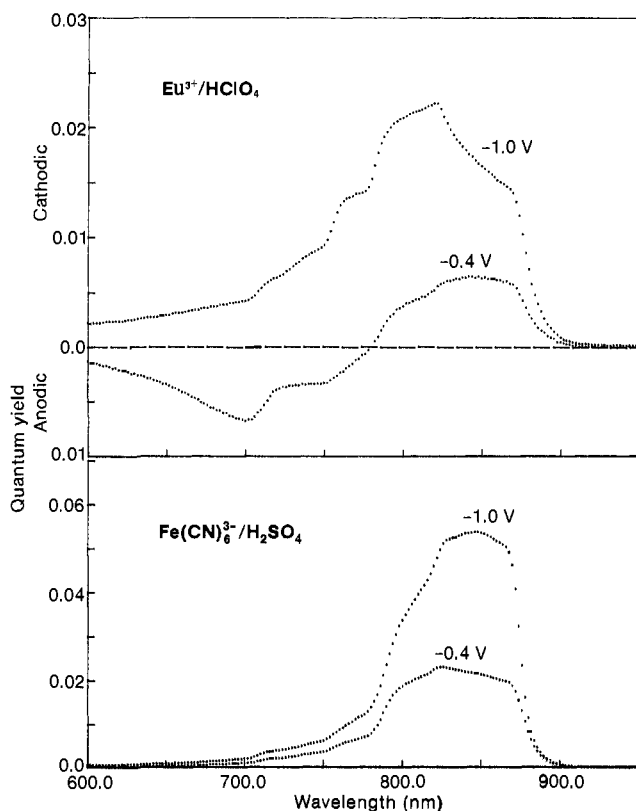
Figure 4. Effect of electrode potential and redox couple on the photocurrent spectra of a $GaAs/GaAs_{0.5}P_{0.5}$ SLS electrode.

Figure 5. Dependence of photocurrent spectra of $GaAs/GaAs_{0.5}P_{0.5}$ SLS electrodes on barrier thickness.

Figure 6. Theoretical energy level scheme for $GaAs/GaAs_{0.5}P_{0.5}$ SLS with 250 Å well and barrier widths. The allowed $\Delta n = 0$ transitions are shown as well as one nonallowed transition from $\Delta_h = 7$ to $\Delta_e = 6$.

tential of the Eu^{3+}/Eu^{2+} couple is -0.67 V compared to $+0.45$ V for $Fe(CN)_6^{3-}/Fe(CN)_6^{4-}$. Thus, the Eu^{3+} electron acceptor has much higher lying energy levels (more negative on the SCE scale) that better overlap the higher energy levels in the GaAs conduction band quantum wells compared to $Fe(CN)_6^{3-}$. Also, the density of states for Eu^{3+} increases with higher energy levels in the conduction band quantum well, while that for $Fe(CN)_6^{3-}$ decreases with these higher energy levels. The relative peak intensities for the two spectra obtained with the same SLS electrode but with the two different electron acceptors (a and b in Figure 1) are summarized in Table II. The peak positions are constant (Table I), but the relative intensities of the lower energy peaks compared to the higher energy peaks are much higher for the $Fe(CN)_6^{3-}$ electron acceptor. In all our samples the absolute magnitude of the quantum efficiency for the $Fe(CN)_6^{3-}$ electron acceptor was significantly higher than that for Eu^{3+} (by about a factor of 2).

At more positive potentials the differences between $Fe(CN)_6^{3-}$ and Eu^{3+} are even more pronounced. In Figure 4, a comparison is made of the photocurrent spectra at -1.0 and -0.4 V. With $Fe(CN)_6^{4-}$ present, the photocurrent is cathodic at all wavelengths at both -1.0 and -0.4 V electrode potentials. With Eu^{3+} present, the photocurrent is cathodic at all wavelengths at -1.0 V electrode potential but changes sign at ~ 775 nm at -0.4 V electrode potential. Also, at -1.0 V the intensities of the higher energy

transitions relative to the lower energy transitions are much higher when Eu^{3+} is present compared to when $Fe(CN)_6^{3-}$ is present; this is consistent with the results in Figures 1a and 3.

Effect of Barrier Thickness. A $GaAs/GaAs_{0.5}P_{0.5}$ SLS with 250 Å GaAs wells and 50 Å $GaAs_{0.5}P_{0.5}$ barriers was studied to examine the effects of barrier thickness. Figure 5 shows the photocurrent spectrum of such an SLS structure at -1 V in 1 M $HClO_4$; a spectrum of a 250 Å GaAs/250 Å $GaAs_{0.5}P_{0.5}$ SLS is also shown under the same conditions. A thick barrier SLS sample was chosen for comparison which had the same general photocurrent spectral shape as the thin barrier sample. The quantum efficiency of the thinner barrier SLS is about twice that of the thicker barrier.

Discussion

The photocurrent spectra of $GaAs/GaAs_{0.5}P_{0.5}$ SLS electrodes show remarkable structure that arises from the quantization of energy levels for electrons and holes in the potential wells created

in the conduction and valence bands of GaAs. We have estimated a theoretical energy level scheme for the 250 Å GaAs/250 Å $GaAs_{0.5}P_{0.5}$ SLS that is shown in Figure 6. The theoretical scheme is derived from the prior calculations of Gourley and Biefeld[7] for the same SLS composition; the calculations include effects of layer strain. We assumed that the spacings of the $\Delta n = 0$ transitions are described by the expression

$$\Delta E \ (1,1 \rightarrow n_h, n_e) = K \left[\frac{n_e^2 - 1}{m_e^*} + \frac{n_h^2 - 1}{m_h^*} \right] \qquad (1)$$

where K is a proportionality constant; n_e and n_h are the quantum numbers for the electron and hole states in the conduction and valence band wells, respectively; m_e^* and m_h^* are the effective masses for electrons and holes; and $\Delta E(1,1 \rightarrow n_h,n_e)$ is the difference in energy between the lowest transition ($n_h = 1$ to $n_e = 1$) and the successively higher n_h to n_e transitions with the same electron and hole quantum numbers. For optical transitions in SL quantum wells, quasiselection rules dictate that the strongest transitions are for $\Delta n = 0$ (2).

A complication for $GaAs_{0.5}P_{0.5}$ is that there are heavy and light hole states with different effective masses. For strained lattices these states are better designated by their angular momenta J and m_J rather than by the terms heavy and light;[7] for the present system these hole states are $|^3/_2, ^3/_2\rangle$ and $|^3/_2, ^1/_2\rangle$, respectively.[7] At room temperature only transitions involving the $|^3/_2, ^3/_2\rangle$ hole states have been reported in the luminescence spectra. These are the transitions that are presented in Figure 6.

The average experimental values of the photocurrent peak positions obtained from the fits of the 4 spectra in Figures 1 and 3 at -1.0 or -0.8 V are presented in Table I. There is good agreement between the theoretical optical transitions with $\Delta n = 0$ and the experimental photocurrent peaks, except for the observed transition at 1.77 eV. The latter corresponds very well to the $\Delta n = 1$ transition between $n_h = 6$ and $n_e = 7$. Such exceptions to the $\Delta n = 0$ selection rule have also been observed in luminescence data.[7] Thus, the photocurrent structure correlates very well with the expected energy level scheme for the SLS quantum wells.

For pure optical absorption processes in superlattices, the absorption coefficient is expected to exhibit a stepwise increase with increasing photon energy, with exciton peaks associated with each step.[2] However, the photocurrent spectra in Figures 1–3 fit very well to a sum of Gaussian peaks. We attribute this behavior to the fact that the photocurrent reflects a combination of photon absorption and photoinduced charge carrier transport processes. The distribution of acceptor states in solution is a broad Gaussian, and we expect that the convolution of the stepwise absorption characteristic with the probability distribution for charge transfer will produce a modification of the step-like absorption spectra. However, further work is required to understand the Gaussian shape of the photocurrent peaks.

The photocurrent spectra sometimes exhibit rather sharp peaks at certain energies that we associate with effects arising from excitonic absorption. Exciton formation is followed by their dissociation and transport of the electrons through the SLS to the acceptor species in the electrolyte. Excitonic structure in optical absorption spectra have been reported for superlattices at room temperature.[15]

From the results presented in Figures 1–5 we propose the following qualitative model for the behavior of $GaAs/GaAs_{0.5}P_{0.5}$ electrodes in photoelectrochemical cells: (1) photoexcitation of the energy levels in the quantum wells occurs with photon energies <1.8 eV (wavelengths >685 nm); (2) with sufficiently negative electrode potential (0.0 to -1 V vs. SCE depending upon the redox potential of the electron acceptor and the electrode sample) this excitation results in net electron transfer from the electron well states into the electrolyte, producing a cathodic photocurrent; the electron transfer is believed to occur from all the photoexcited states and not just from the lowest $n_e = 1$ state; (3) at sufficiently positive potentials ($\sim$0.0 to +0.5 V depending upon electrolyte and electrode sample) net hole transfer from photoexcited hole states in the hole wells occurs producing an anodic photocurrent;

this anodic current has not been identified but is probably oxide formation at the surface of the electrode; (4) there is a competition between electron and hole currents from the respective quantum wells, and at intermediate electrode potentials (about -0.4 eV) the sign of the net photocurrent may depend upon which quantum states are excited; because of the lower mobility of holes, lower energy excitations favor electron transfer out of the wells, while higher energy excitations are required to promote hole transfer from near the top of the hole wells; (5) kinetically fast electron acceptors in the electrolyte shift the photocurrent competition toward the cathodic process so that the cathodic photocurrent dominates at more positive electrode potentials and at shorter wavelengths compared to kinetically slower electron acceptors; (6) at photon energies >1.8 eV mobile electrons and holes are created by excitation processes in the continuum above the wells or in the barrier rather than in the quantum wells; (7) this excitation does not have structure associated with it, but rather it is a smooth function of the wavelength; the sign of this photocurrent depends upon the electrode potential but the transition wavelength where the structured photocurrent appears is independent of potential.

A critical feature of our model is electron transfer to the electrolyte out of higher states in the electron quantum well. The evidence for this is the large variation in relative peak intensities of the photocurrent spectra depending upon the redox potential of the electron acceptor in solution (see Figures 1a, 3, and 4). As seen in Table II, the higher lying (more negative vs. SCE) electron acceptor Eu^{3+} produces much greater photocurrent peak intensities for the higher energy transitions *relative* to the lower energy transitions than does the lower lying $Fe(CN)_6^{3-}$ electron acceptor. These results are explained by the fact that since the Eu^{3+} acceptor has such a negative redox potential it has an energy distribution in the electrolyte relative to the quantum well that increases with energy (i.e., the peak of its Gaussian distribution is above the bottom of the electron quantum well), while the energy distribution of the more positive $Fe(CN)_6^{3-}$ redox acceptor decreases with energy (i.e., the peak of its Gaussian distribution is below the bottom of the electron quantum well). If the electrons were thermalized and hence were being transferred from only one energy level, then the relative intensities of the photocurrent peaks would be independent of the redox potential of the electron acceptors in solution. A detailed study of this effect is in progress.

In the experiments using Eu^{3+} in $HClO_4$ as the electron acceptor, the possibility exists that the H_2 evolution reaction occurs in parallel with Eu^{3+} reduction. Since the initial step for H_2 evolution on GaAs also has a highly negative redox potential, the conclusions discussed above are valid whether the electron acceptor is Eu^{3+} or H^+ or whether both reduction reactions occur together.

It is also to be noted that the absolute quantum efficiencies for reduction of ferricyanide are consistently higher than those for Eu^{3+} or H^+ (see Figures 2–4). This is because the kinetics of charge transfer to $Fe(CN)_6^{3-}$ are much greater than that for Eu^{3+} or H^+;[16] thus, even though Eu^{3+} or H^+ may have better energy overlap with the electron quantum wells the absolute kinetics of reduction are not as good as $Fe(CN)_6^{3-}$. The possibility of strong specific adsorption of $Fe(CN)_6^{3-}$ on the GaAs surface is also a possible factor in this behavior.

The higher quantum efficiencies for $Fe(CN)_6^{3-}$ compared to Eu^{3+} under comparable experimental conditions indicate that the observed photocurrents are not totally limited by light intensity or carrier transport in the electrode. This condition is required in order for our explanation of the origin of the differences in relative peak intensities for high and low energy transitions for different electron acceptors to be valid.

The variation in photocurrent peak intensities with different samples that show approximately constant peak positions is also consistent with electron transport within the SLS occurring from higher states in the wells. As seen in Figure 1b, some samples

(15) J. S. Weiner, D. S. Chemla, D. A. B. Miller, T. H. Wood, D. Sivco, and A. Y. Cho, *Appl. Phys. Lett.*, **46**, 619 (1985).

(16) B. Behr, Z. Borkowska, and H. Elzanowska, *J. Electroanal. Chem.*, **100**, 853 (1979). Z. Borkowska and H. Elzanowska, *Ibid.*, **76**, 287 (1977).

7810 *J. Am. Chem. Soc., Vol. 107, No. 26, 1985*

Nozik et al.

exhibit spectra that are even missing some of the photocurrent peaks; this behavior must be associated with the charge transport. We expect that photocurrent resulting from electron transport from only ground-state levels within the SLS would show the same spectral shape for different samples with the same well width; variations should only occur in the absolute quantum efficiencies.

Electron transfer into the electrolyte from high-lying quantum states in the electron wells means that the electrons are not fully thermalized and that the process therefore involves hot electrons. We have been studying hot electron injection processes in illuminated semiconductor–electrolyte systems[17-20] and have observed the effect in high-doped p-GaP and p-InP bulk semiconductor crystals. The superlattice structures provide an excellent potential system for creating and enhancing hot charge carrier injection processes at semiconductor–electrolyte interfaces. Finally, recent measurements of hot electron relaxation times in photoexcited SL and MQW structures[21-23] show that the thermalization times are greatly increased (one to several orders of magnitude). These results are consistent with the evidence reported here for hot electron injection from $GaAs/GaAs_{0.5}P_{0.5}$ SLS electrodes since longer thermalization times mean that the probability for hot electron injection is increased.

One major question concerning our results is the mechanism of electron transport through the superlattice structure. The 250-Å width of the $GaAs_{0.5}P_{0.5}$ barrier in our initial samples should inhibit tunnelling between wells and make the structure behave as multiple quantum wells; under these conditions one would not expect significant charge transport. However, the relatively large maximum quantum efficiencies (2–12%) shown in Figures 1–4 for the 250-Å barrier SLS indicates significant electron transport perpendicular to the semiconductor layers; the data are consistent with a diffusion length of ~0.05 μm in the perpendicular direction. The origin of this transport has not yet been definitely established; possibilities are thermionic emission over the barriers, field-assisted tunnelling, and defect-assisted tunnelling. The latter could arise from a high density of states created in the forbidden gap of the barrier by a large dislocation density present in the SLS. This proposed mechanism is supported by the results in Figure 5 which show that the 50-Å barrier SLS has twice the quantum efficiency of the 250-Å barrier SLS. Additional studies are required to understand the transport mechanism with more certainty.

Our conclusion that photocurrent is generated from photoexcitation into the continuum of the superlattice at energies >1.8 eV appears to be inconsistent with the 2.0-eV bandgap associated with $GaAs_{0.5}P_{0.5}$. This discrepancy could be explained in two ways: (1) a sub-gap response is present in the barrier that arises from a high density of defect states in the gap; or (2) the barrier layer has a lower phosphorus content than expected from the calibration of the MOCVD apparatus resulting in a smaller band gap. The former explanation would be consistent with the proposed mechanism for charge transport through the barriers. With reference to the latter mechanism, analyses of the superlattice samples with electron microprobe techniques do indicate a lower average phosphorus content, but not sufficiently lower to produce a 1.8-eV bandgap in the barrier layer. Further work is required to explain the photocurrent transition at 1.8 eV.

The falloff in quantum efficiency in the photocurrent tail (photon energies >1.8 eV) for some SLS samples (Figures 1a,b,

2a, 3–5) is attributed to enhanced recombination resulting from excitation that generates free holes and free electrons. Another factor contributing to lower quantum efficiencies at higher energies is that these photons are absorbed closer to the outer surface layers where SEM micrographs show higher degrees of layer distortion; this leads to enhanced recombination processes at the higher density of defects. That severe reduction in quantum efficiency at excitation energies outside the quantum wells is not an intrinsic property of superlattice electrodes is evident in Figures 1c and 2b.

Conclusion

Strained-layer superlattices of $GaAs/GaAs_{1-x}P_x$, $x \approx 0.5$, have been used for the first time as photoelectrodes in photoelectrochemical cells and show pronounced structure in the photocurrent spectra that can be fit by a series of Gaussian peaks. The energies of the peaks correspond very well with the optical transitions expected for the energy level structure for the GaAs quantum wells in the SLS. Samples from different regions of some SLS wafers show marked variations in peak intensities with peak positions being constant within about 0.01 to 0.03 eV.

The photocurrent spectra show a marked dependence on electrode potential and electrolyte redox potentials. At electrode potentials of about –1.0 to –0.8 V vs. SCE, the photocurrent is cathodic at wavelengths from 400 to 950 nm. As the potential is made more positive, the photocurrent changes sign at a wavelength that is dependent upon the electrode potential and the electrolyte redox potential. A more facile electron acceptor, such as $Fe(CN)_6^{3-}$, enhances the cathodic current at higher photon energies compared to kinetically slower redox species, such as Eu^{3+}. At the same electrode potential, the relative intensities of the higher energy photocurrent peaks are much higher compared with the lower energy photocurrent peaks when Eu^{3+} is present in the electrolyte than when $Fe(CN)_6^{3-}$ is present. These results provide strong evidence for hot electron injection into the electrolyte from the high-lying states in the electron quantum wells in the conduction band of GaAs.

$GaAs/GaAs_{0.5}P_{0.5}$ SLS electrodes with 50-Å barriers show about twice the quantum efficiency of those with 250-Å barriers. This is consistent with our belief that charge transport processes through the barrier are important.

From our results we propose the following qualitative model for the photoelectrochemistry of superlattice electrodes: (1) at sufficiently negative electrode potentials, photoexcitation of the quantum wells results in electron transport through the superlattice and into the electrolyte from the higher lying, as well as the lower lying, energy levels in the electron wells; (2) at more positive electrode potentials holes are injected into the electrolyte from hole wells; the competition between net electron or net hole transfer from the illuminated superlattice depends upon the photon energy and electrode potential; lower photon energies and more negative electrode potentials favor net electron transfer from the superlattice; (3) photoexcitation of the superlattice continuum produces photocurrent that does not show structure due to quantization; (4) excitation in the continuum produces free holes that can result in lower quantum efficiencies because of enhanced recombination. This effect is not intrinsic to superlattices, however.

Superlattice electrodes provide a potential system for producing hot electron processes that could lead to high solar photoconversion efficiencies. Important questions remaining to be answered include the mechanism of charge transport through the superlattice, the energy distribution of injected electrons or holes into the electrolyte from the superlattice, and the nature of the potential distribution in the superlattice electrodes and its flatband potential.

(17) G. Cooper, J. A. Turner, B. A. Parkinson, and A. J. Nozik, *J. App. Phys.*, **54**, 6463 (1983).
(18) J. A. Turner and A. J. Nozik, *Appl. Phys. Lett.*, **41**, 101 (1982).
(19) A. J. Nozik, D. S. Boudreaux, and A. J. Nozik, *J. Appl. Phys.*, **51**, 2158 (1980).
(20) R. T. Ross and A. J. Nozik, *J. Appl. Phys.*, **53**, 3813 (1982).
(21) Z. Y. Xu and C. L. Tang, *Appl. Phys. Lett.*, **44**, 692 (1984).
(22) Y. Masumoto, S. Shionoya, and H. Kawaguchi, *Phys. Rev. B*, **29**, 2324 (1984).
(23) J. F. Ryan, R. A. Taylor, A. J. Turberfield, A. Maciel, J. M. Worlock, A. C. Gossard, and W. Wiegmann, *Phys. Rev. Lett.*, **53**, 1841 (1984).